Advanced Robotics, Vol. 20, No. 7, pp. 783–805 (2006)

Also available online - www.vsppub.com

Full paper

Second generation pleated pneumatic artificial muscle and its robotic applications

BJÖRN VERRELST *, RONALD VAN HAM, BRAM VANDERBORGHT, DIRK LEFEBER, FRANK DAERDEN and MICHAEL VAN DAMME

Department of Mechanical Engineering, Vrije Universiteit Brussel, Pleinlaan 2, 1050 Brussels, Belgium

Received 31 May 2005; accepted 31 July 2005

Abstract—This paper reports on the second generation of the pleated pneumatic artificial muscle (PPAM) which has been developed to extend the lifespan of its first prototype. This type of artificial muscle was developed to overcome dry friction and material deformation which is present in the widely used McKibben muscle. The essence of the PPAM is its pleated membrane structure which enables the muscle to work at low pressures and at large contractions. There is growing interest in this kind of actuation for robotics applications due to its high power to weight ratio and adaptable compliance, especially for legged locomotion and robot applications in direct contact with a human. This paper describes the design of the second-generation PPAM, for which specifically the membrane layout has been changed. In terms of this new layout the mathematical model, developed for the first prototype, has been reformulated. This paper gives an elaborate discussion on this mathematical model that represents the force generation and enclosed muscle volume. Static load tests on some real muscles, which have been carried out in order to validate the mathematical model, are then discussed. Furthermore, two robotic applications are given which successfully use these pneumatic artificial muscles. One is the biped Lucy and the another one is a manipulator application which works in direct contact with an operator.

Keywords: Compliant actuation; pneumatic artificial muscle; mathematical modeling.

1. INTRODUCTION

A pneumatic artificial muscle (PAM) is essentially a volume, enclosed by a reinforced membrane, that expands radially and contracts axially when inflated with pressurized air. Thereby, the muscle generates a unidirectional pulling force along the longitudinal axis. When neglecting the membrane's material deformation and

*To whom correspondence should be addressed. Tel.: (32-2) 629-2863. Fax: (32-2) 629-2865. E-mail: bjorn.verrelst@vub.ac.be

the low inertial muscle properties, the generated force is expressed as [1–3]:

$$F = -p\frac{\mathrm{d}V}{\mathrm{d}l}, \tag{1}$$

with p the gauge pressure inside the muscle, $\mathrm{d}V$ the enclosed muscle volume changes and $\mathrm{d}l$ the actuator length changes. The volume of the actuator increases with decreasing length until a maximum volume is reached. At maximum contraction these forces become zero; at low contraction these forces can be very high. Figure 1 gives the working principle of a PAM at constant pressure.

The changing force as a function of contraction at constant pressure is essentially different compared to standard pneumatic cylinders, for which the generated force does not change at constant pressure. For these devices the generated force is proportional to the piston area on which the internal pressure works; consequently, the force does not change with piston position at constant pressure.

Depending on the geometry and type of membrane, the specific force characteristic alters. Several concepts of PAM have been developed over time: some examples are the Romac muscle [4] the Baldwin muscle type [5] and more recently a muscle with Kevlar reinforced fibers developed in Japan [6]. The best-known artificial muscle type is the so called McKibben muscle. This muscle was introduced by McKibben for orthotic applications in the 1950s [7]. Several forms of this type of muscle have actually been commercialized by different companies such as Bridgestone Co. [8], the Shadow Robot Co. [9], Merlin Systems Corp. [10] and Festo [11]. Interest for these actuators is growing, and several groups all over the world use McKibben-like muscles in various robotic and medical applications [12–21].

The concept of the McKibben muscle is given in Fig. 2. It contains a rubber inner tube which will expand when inflated, while a braided sleeving transfers tension. Inherent to this design are dry friction between the netting and the inner tube, and deformation of the rubber tube. Typical working pressure values range from 1

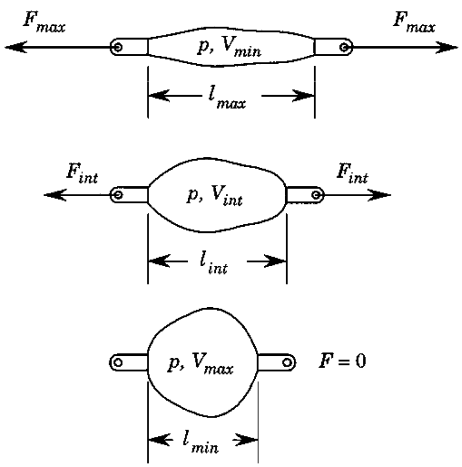

Figure 1. Working principle of a pneumatic artificial muscle [2].

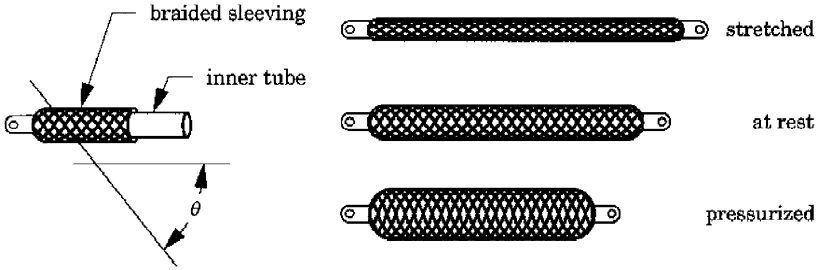

Figure 2. Drawing of the McKibben-type muscle [2].

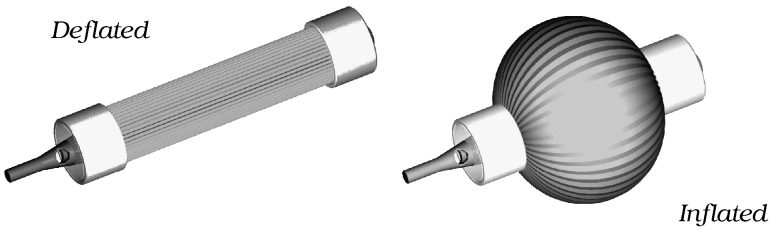

Figure 3. CAD drawing of the deflated and inflated state of the PPAM.

to 5 bar and more. Due to a threshold of pressure which depends on the rubber characteristics, these muscles do not function properly at low pressures.

To avoid friction and deformation of the rubber material, the pleated PAM (PPAM) has been designed by Daerden [2, 3] at the Department of Mechanical Engineering of the Vrije Universiteit Brussel. The membrane of this muscle is arranged into radially laid out folds that can unfurl free of radial stress when inflated. Figure 3 shows the working principle of the PPAM.

The membrane is a fabric made of an aromatic polyamide such as Kevlar to which a thin liner is attached in order to make the membrane air-tight. The high tensile longitudinal fibers of the membrane transfer tension, while the folded structure allows the muscle to expand radially. The folded membrane is positioned into two end-fittings which close the muscle and provide tubing to inflate and deflate the enclosed volume. The end-fittings are constructed with a circular inner teeth structure to position and align each fold of the membrane, while an outer aluminum ring prevents the membrane expanding at the end-fittings. An epoxy resin fixes the membrane to the end-fittings.

Due to its specific design, the PPAM can easily work at pressures as low as 20 mbar. For lifetime considerations of the membrane, the upper limit of the working pressure is set to a maximum 4 bar gauge pressure. Muscle contraction can be more than 40%, depending on the original dimensions (theoretically 54% for a infinitely thin muscle). The muscle prototype built by Daerden [2, 3] has a weight of about 100 g and can generate forces up to 5 kN.

2. PPAM: IMPROVED DESIGN

One of the drawbacks of the first PPAM prototype is its limited lifetime. In Daerden's work, the PPAM design focused on improving the muscle performance, while studying basic control techniques for an unloaded rotative joint. However, extensive usage of the muscles, e.g., as an actuator for a bipedal walking robot, was not immediately considered. For any experimental platform the lifespan of the muscle is obviously crucial. Apart of the interesting scientific aspects related to a study of the PPAM, such a muscle will be economically lucrative if it can be produced at a reasonable price and has a sufficient lifespan.

2.1. Second-generation PPAM

One of the causes of the limited muscle lifespan is the overlap used to make a cylindrical pleated membrane. The membrane of the former prototype is folded while starting from a flat woven fabric. The result of the folding process was a flat pleated membrane; to create a circular shape, one or two folds are glued together with an overlap. During operation, stresses on the interface between the two overlapped membrane pieces create weakened attachments. The pressurized air finds its way through these weakened spots, which results in leakage. To avoid this, the folding production process was changed. Instead of the folded overlap, the folding now starts from an airtight cylindrical fabric in which the folds are created afterwards.

The toothed inner metal tube of the end-fittings of the original prototype requires a lot of machining. Additionally, a large amount of operations are required to position the pleated membrane, fold by fold, in the tooth holes. The idea is to replace this complex end-fitting by a straightforward aluminium basin in which the membrane is fixed by the same epoxy resin. The folds are not deliberately aligned, but are assumed to lie already parallel after the improved folding process. The epoxy keeps the pleated membrane in place.

One of the major changes is made to the membrane layout itself. The most important reason for a shorter lifespan was an incorrect bulging of the pleated membrane. In Fig. 3 the folds are assumed to unfold evenly, but for a real muscle this was hardly the case. It was seen that the membrane is not evenly unfolding, which causes extra parallel stresses on the Kevlar fabric and its airtight coating, especially at the top of each fold. It was observed that the axial Kevlar fibers on each top tend to move towards the bottom of their respective crease, leaving a gap at the top. This of course weakens these spots and allows the pressurized air to leak. As a solution to this the membrane composition is changed by only using high-tensile stiffness fibers positioned at the bottom of each crease, while another more flexible fabric is used to create the folded membrane structure and keep the pressurized air inside the muscle. The flexible fabric is a simple woven polyester cloth, which is made airtight by a polymer liner. This structure is folded and in each crease a yarn of high-tensile Kevlar fibers is responsible for transferring the large

axial tension. Figure 4 depicts the complete straightforward construction of the new muscle.

In contrast to the former design, this muscle prototype does not incorporate air connectors. The end-fittings have a treated hole in which additional muscle connectors can be screwed. An advantage of this setup is that a broken muscle can be replaced easily, without having to change the more complex muscle connectors. These connectors incorporate three functions: guiding the pressurized air in and out the enclosed volume, creating the interface for the connection to the specific application frame, and providing an attachment for a pressure sensor positioned inside the muscle. Figure 5 shows the two different connectors to be fixed at each side of the muscle.

The left-side drawing of Fig. 5 shows the connector which allows the air to flow in and out of the muscle, while the right-side drawing depicts the connector with the attachment for a pressure sensor. Both connectors are made of aluminum and have

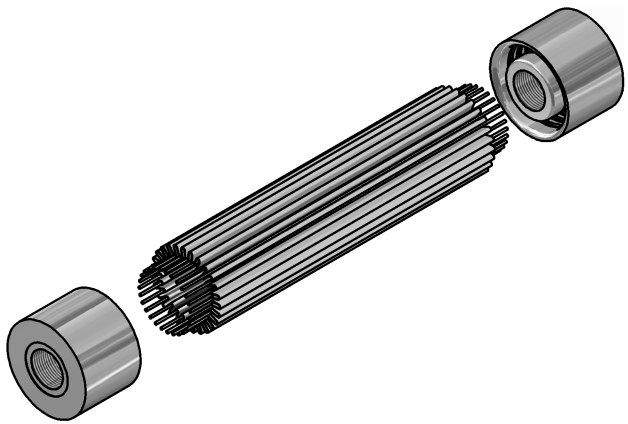

Figure 4. Composition of the new muscle prototype.

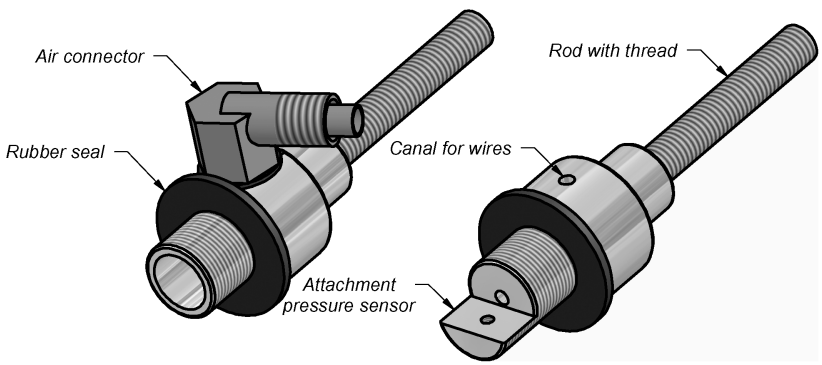

Figure 5. Drawing of the two muscle end-connectors.

Figure 6. Photograph of inflated state of the second-generation PPAM.

a rubber sealing. At the back of each connector a threaded rod forms the interface to the application frame. A standard air tube connector can be fixed in the muscle connector on the left of Fig. 5. A small borehole has been drilled in the muscle connector for the pressure sensor to guide the wires of the electronics needed for the pressure sensor, which is positioned inside the muscle. Once this sensor and its wiring are positioned, the borehole is filled with epoxy resin to prevent the air from escaping from the enclosed volume.

Finally, Fig. 6 shows a photograph of the new muscle prototype. The muscle is shown in its inflated state. Note the regular unfolding of the flexible membrane while the Kevlar fibers stay positioned at equal distances. A lifespan test was performed, in which a muscle moves up and down a load of 130 kg by a slow varying gauge pressure between 1 and 3 bar. About 400 000 cycles were reached before the test was ended. At this large number of cycles a few Kevlar fibers were broken somewhere in the end-fittings. The epoxy resin makes the fibers fragile at these spots. Although movements of the fibers in the end-fittings are small, the fibers will break eventually due the large number of cycles.

2.2. Mathematical model

In this section, the mathematical model describing the muscle characteristics, developed by Daerden [2, 3], is adapted according to the new membrane design. The original model assumed a continuous axisymmetrical circular membrane, while for this model the focus lies on the discrete number of high-tensile longitudinal fibers. The initial assumptions of the model are different, but the resulting analytical solution is almost identical. Therefore, only the starting point for the model is established here, while the elaboration on the analytical solution can be found in Ref. [2]. This PhD text can be found at http://lucy.vub.ac.be/publications.htm. For convenience, a list of nomenclature can be found in Table 1.

Table 1.
Nomenclature

β	oriented angle between $\bar{1}_r$ and $d\bar{F}_p$	rad
ϵ	muscle contraction	
σ	tensile stress	Pad
φ	elliptical integral amplitude	rad
c_i	constant transformation parameter i	
dA	elementary surface associated with w and dL	m^2
dL	infinitesimal muscle fiber length	m
$E(\varphi \setminus m)$	elliptical integral of the first kind	
$F(\varphi \setminus m)$	elliptical integral of the second kind	
F	generated force amplitude	N
$\bar{F}_p$	force transferred by muscle membrane	N
$\bar{F}_t$	muscle traction force	N
$f\left(\epsilon, \frac{l_0}{R}\right)$	dimensionless muscle force function	
f_i	coefficients of a polynomial force fitting	
l	muscle/fiber length	m
l_o	initial muscle/fiber length	m
m	elliptical integral parameter	
n	number of used fibers	
p	gauge pressure inside muscle	bar
r	radial distance from fiber to central muscle axis	m
R	unpressurized muscle radius	m
s	fiber section	m^2
w	half the distance between two neighboring fibers	m
$v\left(\epsilon, \frac{l_0}{R}\right)$	dimensionless volume function	
v_i	coefficients of polynomial muscle volume fitting	
V	enclosed muscle volume	m^3
$\bar{1}_r$	unity vector corresponding radial direction	
$\bar{1}_x$	unity vector corresponding axial direction	

A meridional and parallel section of the new muscle is given in Fig. 7. The muscle is pressurized and subjected to a longitudinal traction force $\bar{F}_t$. For the mathematical formulation it is assumed that longitudinal tension is only transferred by the high-tensile fibers which are positioned in each crease. Any influence of the more flexible longitudinal fibers of the airtight polyester membrane is thus neglected. The membrane transfers the forces $\bar{F}_p$ that are generated on it by the pressurized air to the high-tensile longitudinal fibers. A three-dimensional view of an infinitesimal section of the membrane is depicted in Fig. 8 with the forces acting on the longitudinal fiber.

At the left and right side of the fiber, part of the membrane transfers a force $d\bar{F}_{p*}$. Due to the axisymmetrical situation of the closing membrane, the parallel components of these forces, which are tangent to the perpendicular circle running through the longitudinal fibers, compensate for each other. Consequently, only the

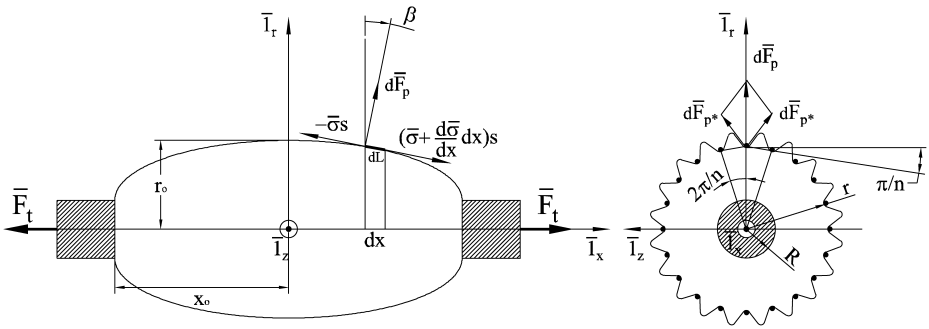

Figure 7. Meridional and parallel view of the PPAM.

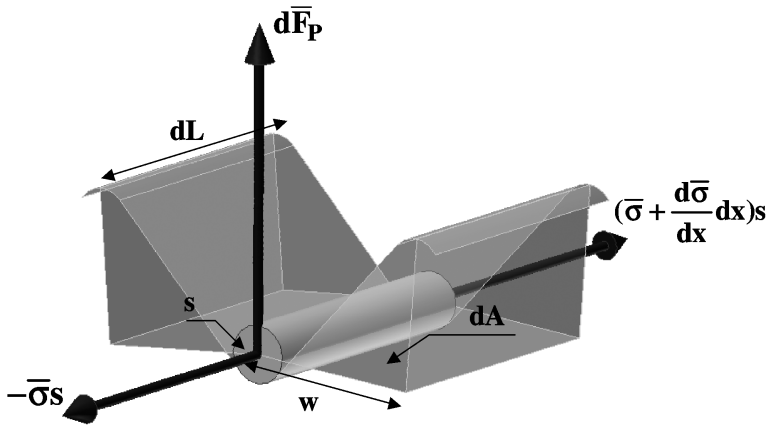

Figure 8. Three-dimensional view of an infinitesimal section of the membrane.

resultant force, $\mathrm{d}\bar{F}_\mathrm{p}$, is taken into account. The magnitude of this is calculated as:

$$\left|\mathrm{d}\bar{F}_\mathrm{p}\right| = 2p\cos\frac{\pi}{n}\mathrm{d}A = 2pw\cos\frac{\pi}{n}\mathrm{d}L, \tag{2}$$

with p the gauge pressure inside the enclosed volume, n the number of longitudinal fibers, evenly distributed over the membrane, w representing half the distance between two neighbouring longitudinal fibers, and $\mathrm{d}A$ the elementary surface associated with w and the infinitesimal section length $\mathrm{d}L$. If β defines the oriented angle (counter-clockwise positive) between the radial direction $\bar{\mathrm{l}}_\mathrm{r}$ and the force vector $\mathrm{d}\bar{F}_\mathrm{p}$, the components of this vector are represented by:

$$\mathrm{d}\bar{F}_\mathrm{p} = \left(-2pw\cos\frac{\pi}{n}\mathrm{d}L\sin\beta\right)\bar{\mathrm{l}}_x + \left(2pw\cos\frac{\pi}{n}\mathrm{d}L\cos\beta\right)\bar{\mathrm{l}}_\mathrm{r} \tag{3}$$

$$= \left(-2pr\sin\frac{\pi}{n}\cos\frac{\pi}{n}\tan\beta\mathrm{d}x\right)\bar{\mathrm{l}}_x + \left(2pr\sin\frac{\pi}{n}\cos\frac{\pi}{n}\mathrm{d}x\right)\bar{\mathrm{l}}_\mathrm{r} \tag{4}$$

$$= \left(-pr\sin\frac{2\pi}{n}\tan\beta\mathrm{d}x\right)\bar{\mathrm{l}}_x + \left(pr\sin\frac{2\pi}{n}\mathrm{d}x\right)\bar{\mathrm{l}}_\mathrm{r}. \tag{5}$$

Thus, using following transformations:

$$\cos\beta = \frac{\mathrm{d}x}{\mathrm{d}L}, \tag{6}$$

$$w = r\sin\frac{\pi}{n}, \tag{7}$$

with r the radial distance from the fiber to the central muscle axis $\bar{1}_x$ and $\mathrm{d}x$ the projection of the infinitesimal fiber length $\mathrm{d}L$ on to the same axis.

Assuming the tensile stress σ, generated in the high-tensile longitudinal fiber, is constant over the fiber section s, the force associated with this stress is given by:

$$\bar{\sigma}s = (\sigma s\cos\beta)\,\bar{1}_x + (\sigma s\sin\beta)\,\bar{1}_\mathrm{r}. \tag{8}$$

Shear stresses are neglected since the longitudinal fiber is extremely flexible in the perpendicular direction. If, additionally, the gravitational force associated with the weight of the membrane and high-tensile fibers is neglected with respect to the much higher tensile forces, the equilibrium of forces acting on the infinitesimal fiber piece $\mathrm{d}L$ can be expressed along the directions $\bar{1}_x$ and $\bar{1}_\mathrm{r}$:

$$\bar{1}_x: \qquad -pr\sin\frac{2\pi}{n}\tan\beta\mathrm{d}x + \frac{\mathrm{d}(\sigma s\cos\beta)}{\mathrm{d}x}\mathrm{d}x = 0, \tag{9}$$

$$\bar{1}_\mathrm{r}: \qquad pr\sin\frac{2\pi}{n}\mathrm{d}x + \frac{\mathrm{d}(\sigma s\sin\beta)}{\mathrm{d}x}\mathrm{d}x = 0. \tag{10}$$

Eliminating $pr\sin(2\pi/n)$ from (9) and (10) leads to:

$$\frac{\mathrm{d}(\sigma s\sin\beta)}{\mathrm{d}x}\tan\beta + \frac{\mathrm{d}(\sigma s\cos\beta)}{\mathrm{d}x} = 0. \tag{11}$$

Rearranging the differentials and multiplying (11) with $\cos\beta$ leads to:

$$\frac{\mathrm{d}(\sigma s)}{\mathrm{d}x} = 0, \tag{12}$$

which results in:

$$\sigma s = c, \tag{13}$$

with c an integration constant.

Substituting $\tan\beta = \mathrm{d}r/\mathrm{d}x$ in (9), while integrating gives:

$$\frac{r^2}{2}\,p\sin\frac{2\pi}{n} + c' = \sigma s\cos\beta, \tag{14}$$

with c' an integration constant. Assuming that the traction force F_t is equally distributed over the n different longitudinal fibers, this integration constant can be interpreted as $c' = F_\mathrm{t}/n$ [2].

If the longitudinal high-tensile fibers are assumed to be inelastic (a special case of the discussion in Ref. [2]), the following geometrical constraint on the fiber length

l_0 has to be taken into account:

$$\int_{x=0}^{x=x_0} \mathrm{d}L = \int_{x=0}^{x=x_0} \sqrt{1 + \left(\frac{\mathrm{d}r}{\mathrm{d}x}\right)^2}\,\mathrm{d}x = \frac{l_0}{2}, \tag{15}$$

with x_0 being the extreme ends of the enclosed volume of the muscle. Using the relation $\sqrt{1 + (\mathrm{d}r/\mathrm{d}x)^2} = 1/\cos\beta$ and $c' = F_\mathrm{t}/n$, (14) can be transformed to the following differential equation:

$$\mathrm{d}x = -\frac{c_2 r^2 + c_3}{\sqrt{1 - (c_2 r^2 + c_3)^2}}\mathrm{d}r, \tag{16}$$

with:

$$c_2 = \frac{p \sin\frac{2\pi}{n}}{2\sigma s}, \tag{17}$$

$$c_3 = \frac{F_\mathrm{t}}{n\sigma s}. \tag{18}$$

Given a pressure p and traction F_t, as a consequence of (13), c_2 and c_3 are constant. Finally, the differential equation (16) can be integrated from $x = 0$ to $x(r)$, in order to determine the shape of the curved fibers with each pressure level p and traction F_t. This integration is not straightforward, but has been analytically described by Daerden. Only the solution is repeated here, a detailed discussion can be found in Ref. [2].

For the analytical solution two new constants, m and φ_R were introduced. These relate to c_2 and c_3 as follows:

$$c_2 = 2m\frac{\cos^2\varphi_R}{R^2}, \tag{19}$$

$$c_3 = 1 - 2m, \tag{20}$$

and their values are bounded as $(0 \leqslant m \leqslant 1/2)$ and $(0 \leqslant \varphi_R \leqslant \pi/2)$. The symbol R represents the unpressurized muscle radius. The geometrical representation of the constants m and φ_R is not straightforward. A detailed discussion on this topic is given in Daerden [2].

Defining the muscle contraction ϵ as:

$$\epsilon = 1 - \frac{2x_0}{l_0}, \tag{21}$$

and after introducing the running coordinate φ, the shape of the longitudinal fibers, at contraction ϵ, can be found from the following set of equations:

$$x = \frac{R}{\sqrt{m}\cos\varphi_R}\left(E\left(\varphi \setminus m\right) - \frac{1}{2}F\left(\varphi \setminus m\right)\right), \qquad 0 \leqslant \varphi \leqslant \varphi_R, \tag{22}$$

$$r = \frac{R}{\cos\varphi_R}\cos\varphi, \qquad 0 \leqslant \varphi \leqslant \varphi_R, \tag{23}$$

$$\frac{E\left(\varphi_R \setminus m\right) - \frac{1}{2}F\left(\varphi_R \setminus m\right)}{\sqrt{m}\cos\varphi_R} = \frac{l_0}{2R}\left(1-\epsilon\right), \tag{24}$$

$$\frac{F\left(\varphi_R \setminus m\right)}{\sqrt{m}\cos\varphi_R} = \frac{l_0}{R}, \tag{25}$$

with $E(\varphi \setminus m)$ and $F(\varphi \setminus m)$ elliptical integrals of the first and second kind.

For each contraction ϵ, a combination of the constants m and φ_R has to be calculated from (24) and (25). The two values are found numerically using Newton's rootfinding in a combination of these two equations. A detailed discussion on the derivation of the numerical solution is given in Daerden's work [2]. When these values are found, (22) and (23) fully characterize the shape $x(\varphi) - r(\varphi)$ of the fibers at each contraction. From this set of equations, valid only with the assumption of inelastic fibers, it is seen that the solution is characterized by the muscle slenderness l_0/R. At this point there is no difference with the solution of Daerden, the shape at which the longitudinal fibers position at each contraction ϵ is the same. The difference arises when expressing the force generated with each contraction. This force is dependent on the number of fibers, as is shown in the next section.

2.3. Characteristic of the PPAM

Daerden [2, 3] extensively discusses several characteristics concerning the PPAM, for inelastic as well as elastic membranes. Thus, giving for each contraction the characteristics of the membrane shape, muscle traction, enclosed volume, maximum muscle diameter, and fiber stress and strain values. Here, two important characteristics are discussed: generated traction and enclosed volume for each contraction. The first is used for joint torque dimensioning and control purposes, while the latter can be important for simulation purposes and calculation of joint compliance with closed muscles.

To determine the traction characteristics, (17) and (18) are combined with the parameter transformations (19) and (20):

$$F_{\mathrm{t}} = n\sigma s c_3 = pn\sin\left(\frac{2\pi}{n}\right)\frac{c_3}{2c_2} = pn\sin\left(\frac{2\pi}{n}\right)\frac{\left(1-2m\right)R^2}{4m\cos^2\varphi_R}. \tag{26}$$

Using (24) gives:

$$F_{\mathrm{t}} = pn\sin\left(\frac{2\pi}{n}\right)l_0^2\frac{\left(1-2m\right)\left(1-\epsilon\right)^2}{16\left[E\left(\varphi_R \setminus m\right) - \frac{1}{2}F\left(\varphi_R \setminus m\right)\right]^2} \tag{27}$$

$$= p\frac{n}{2\pi}\sin\left(\frac{2\pi}{n}\right)l_0^2 f\left(\epsilon, \frac{l_0}{R}\right), \tag{28}$$

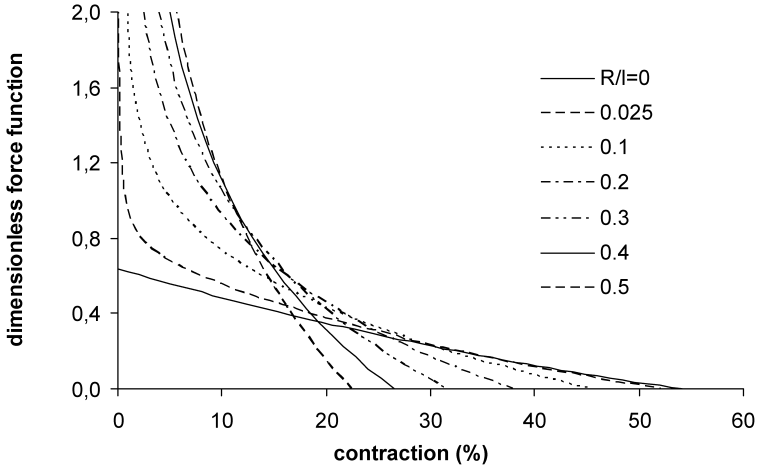

Figure 9. Dimensionless force function.

with $f(\epsilon, l_0/R)$ the dimensionless force function as defined in Refs [2, 3]. This function depends only on contraction and geometry as far as the elasticity of the fibers is neglected. Figure 9 represents the dimensionless force function for different values of broadness R/l. The thicker the muscle, the less it contracts and the higher the forces it generates. Contraction can reach up to 54% in a theoretical case with $R/l = 0$, which is bounded in practise because of minimum space needed to fold the membrane.

Expression (28) shows the difference between the current model and that of Daerden, i.e., a term $(n/2\pi)\sin(2\pi/n)$ appears. This term lowers the generated traction compared to the model of Daerden when the number of fibers is decreased. When increasing the number of fibers, the difference between the traction models becomes smaller. As the number of used fibers (n) increase to infinity, the model should corresponds to the case of a closed circular membrane, as was assumed by Daerden:

$$\lim_{n\to\infty} \frac{n}{2\pi} \sin\frac{2\pi}{n} = 1. \tag{29}$$

Thus, the two models are the same for large numbers of discrete fibers. The limit in (29) converges fast to 1; if the number of used fibers is greater then 15 then the difference between the two models is less then 3%. Generally, if the number of fibers is large enough, the generated muscle force depends on the applied gauge pressure (p), the contraction (ϵ) and the two parameters, initial muscle length (l_0) and slenderness (l_0/R). The latter two are important during the joint design process, where these parameters are chosen as a function of the desired joint torque characteristics.

For the mathematical description of the enclosed volume, the pleated polyester membrane is approximated by considering at each parallel section a circular membrane pattern instead of the pleated structure. These calculations are identical

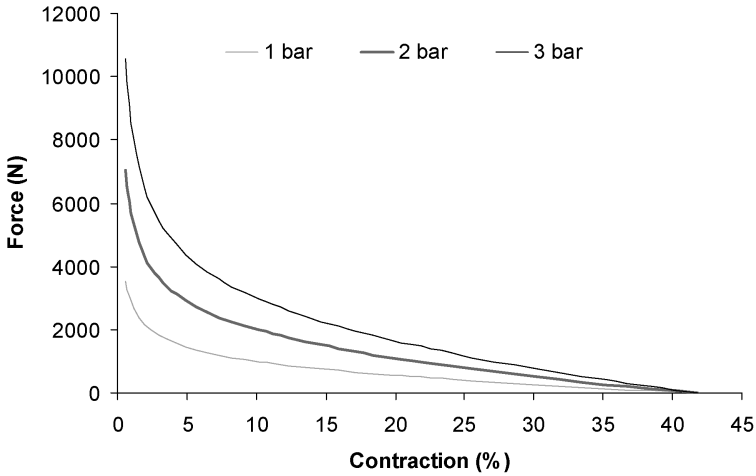

Figure 10. Theoretical forces at pressure levels 1, 2 and 3 bar as a function of contraction.

as in the work of Daerden [2] and resulted in the following expression:

$$V = l_0^3 v\left(\epsilon, \frac{l_0}{R}\right), \tag{30}$$

with v a dimensionless function of the contraction and the slenderness only.

Tested muscles which are currently used for several setups have a physical membrane length $l_0 = 110$ mm, an unpressurized radius $R = 11.5$ mm for the position of the Kevlar fibers and a radius of 16 mm at the top of the polyester fabric pleats. These specific dimensions result from the standard tools used for the fabrication of the muscles and the unloaded radius takes into account the dimensions of the pressure sensor which is positioned inside the muscle. The muscle used for the biped is constructed with 40 aligned fiber yarns. The extra term (29), distinguishing this specific force model, is 0.996 for this number of fibers. Thus, the predicted forces generated by this muscle are almost identical for both models. Using $l_0 = 110$ mm, $R = 11.5$ mm and $n = 40$ in (28) results in the force characteristics depicted in Fig. 10. The traction as a function of contraction is drawn for different applied gauge pressures: 1, 2 and 3 bar.

The graph shows the non-linear character of the generated muscle force. For small contractions, the forces are extremely high; for large contractions, the forces drop to zero. For practical robot application, contractions will be bounded somewhere between 5 and 35%. The first limit is set to bound the stresses on the fibers and consequently extend the lifetime of the muscle. Beyond 35% contraction, forces drop too low to be of practical use. The volume characteristic is given for the considered muscle dimensions in Fig. 11. The volume ranges from a dead volume of approximately 100 ml at zero contraction to a volume of about 400 ml at maximum contraction.

The volumes of the end-fittings and tubing should be added to the dead volume.

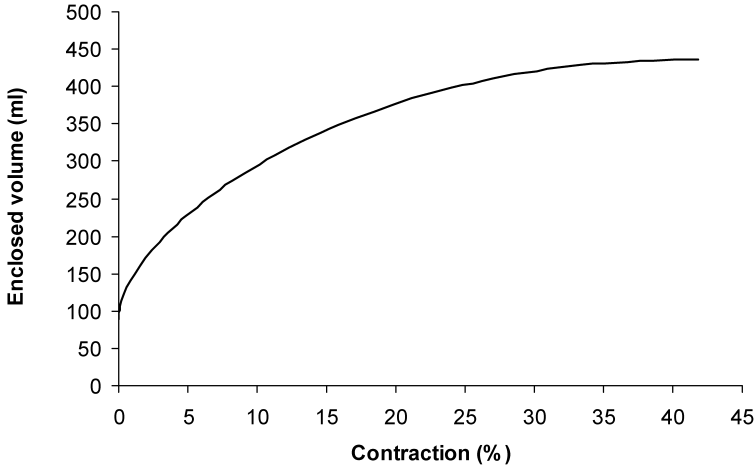

Figure 11. Theoretical enclosed muscle volume as a function of contraction.

3. STATIC LOAD TESTS

Static load tests on real muscles are carried out to validate the proposed mathematical model of (28). Three different muscles are tested with an Intron test bench (model 4505) at isobaric conditions, while applying three different gauge pressures: 1, 2 and 3 bar. The forces are recorded with a load cell of 10 kN (accuracy $\pm$ 0.05%) and the pressure inside the muscle is regulated with a Kolvenbach pressure servo-valve (KPS3/4). In order to increase accuracy, the pressure inside the muscle is separately measured with a silicon gauge pressure sensor (XCA5-60GN; Data Instruments; accuracy $\pm$ 0.5% of 60 p.s.i. span). This sensor is placed as close as possible to the inlet of the muscle. One side of the muscle is fixed to the load cell, while the other side is attached to a movable frame. The tests are performed by changing the displacement of this frame. During each test, the frame position, muscle force and applied gauge pressure are recorded.

For each test, the voltage controlling the servo-valve is set at the beginning of each run to regulate the pressure in the muscle at a constant level. Subsequently, the moving part of the test bench displaces in such a way that the generated force of the muscle ranges between 100 and 3000 N, following a slow sine wave path of 0.005 Hz such that the pressure is stabilized at each measurement. Figure 12 gives the results of these tests by depicting force as a function of contraction for each of the three muscles at the three different gauge pressures.

Although the muscles are handmade, the repeatability is very satisfactory. On the graph, an un-modelled hysteresis effect on the actual force as a function of contraction curve is noticed. It is seen that the different curves show a more or less comparable hysteresis width. Due to the pressure regulating valve, the actual pressure during each test run is not exactly the same. To overcome this, it is better to compare the test results by dividing the measured forces by the measured pressures.

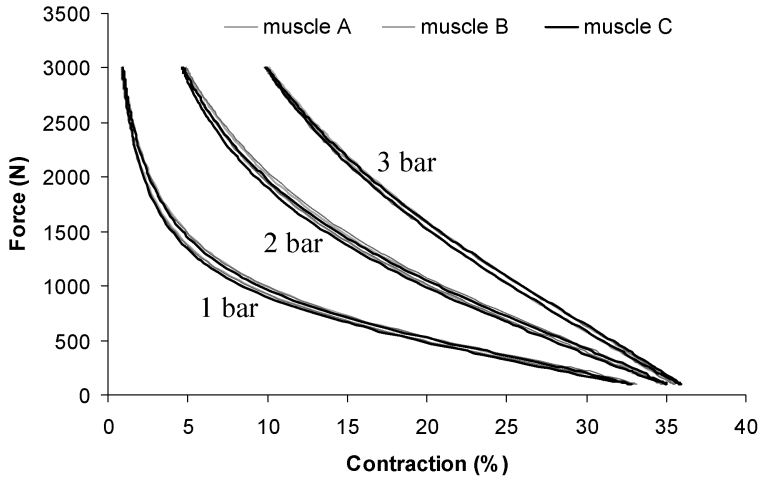

Figure 12. Measured forces as a function of contraction for three muscles at pressure levels 1, 2 and 3 bar.

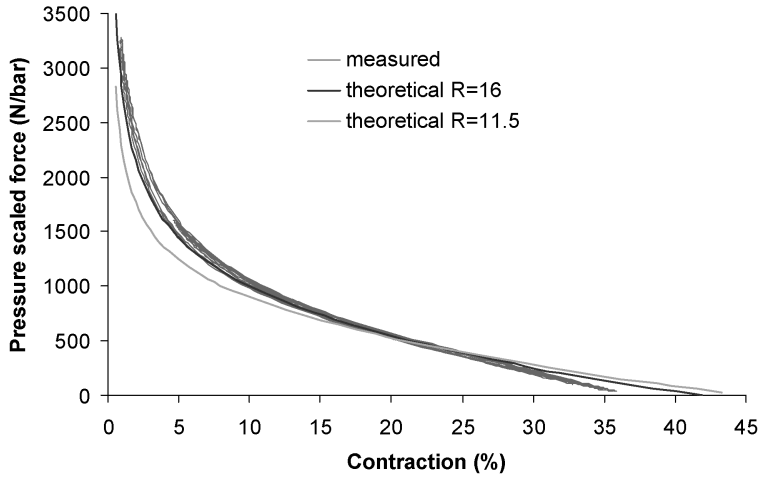

Figure 13. Pressure scaled measured forces as a function of contraction compared with theoretical models.

Figure 13 shows all the pressure scaled measurements together with estimated theoretical force functions of (28). These two theoretical graphs are calculated with $R = 11.5$ mm and $R = 16$ mm respectively. The first compares to the actual radius at which the Kevlar fibers are positioned during construction of the muscles. The radius equal to 16 mm corresponds to the radius of the top of the pleats, which is the same as the outer radius of the enclosed volume at the aluminium end fittings.

It is seen that the theoretical model with $R = 11.5$ mm does not fit the measured data, while the other graph with $R = 16$ mm is much more suited to represent the actual generated force. Since the epoxy resin reaches to only about a centimeter

Table 2.
Coefficients of the polynomial force function approximation

f_4	f_3	f_2	f_1	f_0
−2.041	171.62	−7178.9	128 611	146 099

away from the edge of the end fitting, the Kevlar fibers tend to be positioned at the outer radius of the aluminium basin, immediately after the muscle is pressurized. At all contractions the fibers at the end fittings stay at this radius, as if the initial radius was $R = 16$ mm. This explains why the theoretical function with the larger radius fits the measured data much better. For full bulging of the muscle the initial diameter of the cylindrical polyester membrane should be taken higher then the initial length of the muscle. But it has been observed, for a muscle with not fully unfolded pleats at maximum contraction, that the unfolding process is less regular as with the previous muscle design. So the initial diameter of the cylindrical polyester tube is taken smaller. Consequently, the muscle can not fully bulge and at certain contraction level, radial stresses in the polyester membrane start influencing the traction characteristic. This explains why the theoretical model deviates from the measured data (see Fig. 13) at large contractions.

Since the force functions of the different muscles are very similar, a polynomial function fit on the pressure scaled measured data is performed in order to achieve a better force estimation. The nonlinear nature of the force function attains extremely large values at small contractions, therefore it is more suitable to perform a polynomial fit on the scaled force function multiplied with contraction. This lowers after all the extreme values at small contractions. A fourth-order polynomial fit on these data is performed. With the incorporation of pressure p and the square of the initial muscle length l_0^2, as was described by the theoretical model, the polynomial fit of the force function can be expressed as:

$$F_t = pl_0^2 f(\epsilon) = pl_0^2 \left(f_4\epsilon^3 + f_3\epsilon^2 + f_2\epsilon + f_1 + f_0\epsilon^{-1}\right) \tag{31}$$

with f_0 to f_4 the 5 coefficients resulting from a 4th order polynomial approximation. Figure 14 shows all the pressure scaled force measurements in comparison with the estimated force function.

The coefficients of the fitting process for the force function, following the structure of (31), are given in Table 2. The values are valid when the generated force F_t is expressed in Newtons, the initial muscle length l_0 in meters, the pressure expressed in bars and the contraction ϵ expressed in percent.

Finally, a polynomial fitting is performed on the theoretical data for the enclosed muscle volume depicted in Fig. 11:

$$V(\epsilon) = l_0^3 v(\epsilon) = l_0^3 \left(v_5\epsilon^5 + v_4\epsilon^4 + v_3\epsilon^3 + v_2\epsilon^2 + v_1\epsilon + v_0\right), \tag{32}$$

with v_0 to v_5 being the six coefficients resulting from a fifth-order polynomial approximation. Equation (32) is much easier to handle than the numerical solution

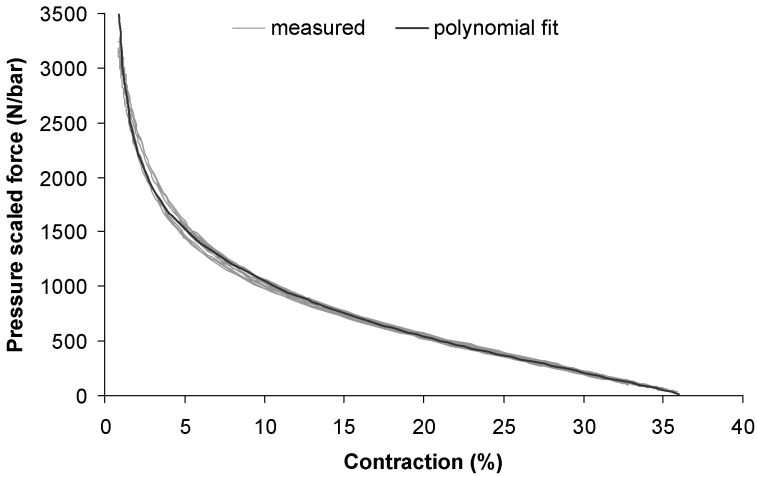

Figure 14. Pressure scaled measured forces as a function of contraction compared with the polynomial fitted estimation.

Table 3.
Coefficients of the polynomial volume function fitting

v_5	v_4	v_3	v_2	v_1	v_0
0.023	−2.63	113.82	−2386.3	30080	71728

derived from the mathematical model represented by expression (30). The coefficients of the volume fitting, following (32) are given in Table 3. The values are valid for the volume given in milliliters, the initial length expressed in meters and the contraction ϵ expressed in percent. The data in Tables 2 and 3, together with (31) and (32), can also be used to generate an approximation of the force and volume characteristics for muscles with lengths different from $l_0 = 110$ mm. However, the values in these tables are only valid for muscles with a specific slenderness ($l_0/R = 110/16 = 6.9$), as explained by the theoretical model with (30) and (28). Thus, whenever the polynomial fitting is used for a muscle with different initial length, the unloaded radius of that muscle has to be adapted, otherwise the force and volume approximations are not valid.

4. APPLICATIONS OF THE PPAM

4.1. The PPAM for legged robots

Not so long ago legged robots were exclusive topics for science-fiction movies and the imagined world of children. However, recent developments indicate that these machines will become full-fledged robots in the near future. One example is the Honda Motor Corp. that developed the Honda Human Robot, followed by

its successors P1, P2 and recently ASIMO. Since Honda is heavily investing in this research domain, it seems to have triggered interest for legged locomotion, resulting in a wide variety of robots built world-wide. Most of these robots use electrical actuation since this type of actuation is available of the shelf and its control principles are well know. Electrical motors generally produce low torques at high rotation speeds, whereas robotic application demand opposite characteristics, thus complex transmission units are generally required. This results in a stiff joint actuation interface which is very beneficial towards high precision position tracking, but has some disadvantages towards legged locomotion. Absorption of impact shocks during touchdown of a leg by the stiff actuation system becomes difficult and exploitation of natural dynamics of the motion is obstructed. The latter means that passive swing motions of the robot limbs during the walking motion are exploited in order to reduce global energy consumption. With respect to these two topics an interesting alternative is given by the use of pneumatic artificial muscles as actuation system for legged robots.

The biped 'Lucy' is a two-dimensional walking robot with two articulated legs and an armless body. This robot has been built to create a test bed for the evaluation of the PPAM implemented for legged locomotion. This research is focused on the exploitation of the adaptable compliance present in a joint actuated by two artificial muscles. One can show that joint position is determined by pressure differences in both muscles, while the stiffness of a joint is characterized by the sum of pressures. This means that stiffness can be changed while still controlling position. The adaptability of compliance is very important with regard to energy consumption and control efforts. The strategy is to select appropriate stiffness parameters in the different joints in order to adapt the natural dynamics of the robot to an imposed desired motion. Moving within the natural dynamics of a system would only need energy to overcome friction, while each motion deviating from this situation would require more energy input and control effort.

Figure 15 shows a picture of Lucy, more information about this biped can be found in Ref. [22] and movies can be viewed at the Lucy website: http://lucy.vub.ac.be/

4.2. The PPAM in a manipulator application

Repetitive manual handling of heavy loads is common in assembly and is a frequent cause of lower back disorders. This can have a significant impact on quality of life and has a serious economic cost. Manipulators are robotic systems designed to avoid these problems. They assist people in performing heavy-duty tasks. Most of the commercially available manipulators use a counterweight, which limits their use to handling loads of a specific mass. Others are electrically or hydraulically actuated. This usually makes them heavy, complex and expensive. The use of the PPAM actuator allows us to tackle these issues, and develop a manipulator that combines ergonomics, operator safety, low cost, low weight and ease of operation.

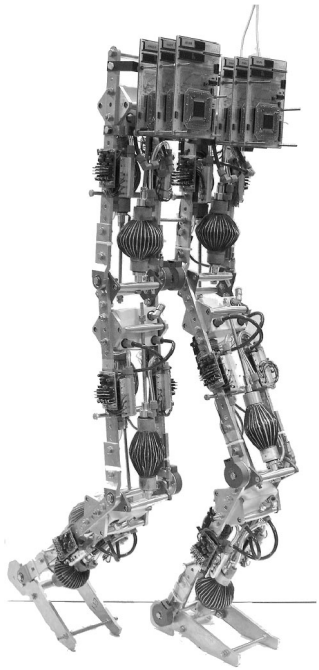

Figure 15. Picture of the robot Lucy, actuated by 12 PPAMs.

The goal of this research is to develop a manipulator that will be used in direct contact with an operator, without expensive force or torque sensors and without user interaction through control elements (such as joysticks). The system should behave as follows: when the operator wants to move a load attached to the manipulator, he/she starts moving it as if there were no manipulator. By measuring the muscle gauge pressures, the system can estimate the forces applied by the operator and assist him in accomplishing the desired load movement. Ideally, moving a 30-kg load would feel like moving a 3-kg load. The direct interaction between operator and load (without intermediary control tools) allows for precise positioning.

The main requirement for any mechanical device that is used in the immediate environment of people is safety. The PPAM actuators greatly contribute to the overall safety of the manipulator system: they allow for a lightweight construction, there is no danger of electrocution and, most important of all, the muscles are inherently compliant. The controller will also enhance safety, since there is no fundamental difference between forces generated by a collision and forces applied by an operator. The system will always tend to move away from people or objects it collides with.

A hardware setup of a small-scale manipulator was constructed. It consists of two PPAM actuated links in inverse elbow configuration. A picture of the manipulator arm is given in Fig. 16.

More information about this research can be found in Ref. [23] and some movies can be found at the website http://werk.vub.ac.be/softarm

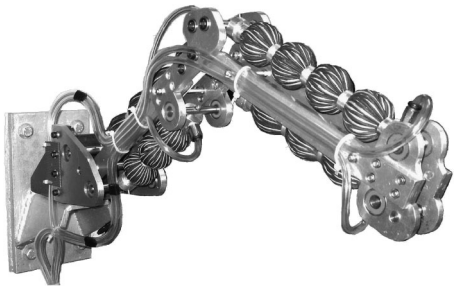

Figure 16. Picture of the manipulator arm, actuated by four PPAMs.

5. SUMMARY

In this paper the PPAM as designed by Daerden was introduced. This type of artificial muscle was developed to overcome dry friction and material deformation observed in the widely used McKibben-type artificial muscle. The essence of the PPAM is its pleated membrane structure which enables the muscle to work at low pressures and at large contractions. In order to deal with some limitations of the PPAM design of Daerden, a second-generation PPAM was proposed. A redesign of the pleated membrane structure resulted in a much higher muscle lifespan, which is an essential property if the muscle is used for an elaborate experimental setup. Additionally, some changes made to the end fitting design simplified machining of the muscle and provided possible reuse of some muscle parts.

The new membrane layout differs from the previous design mainly due to use of a discrete number of high-tensile fibers instead of a complete high-tensile stiff fabric. Therefore, the mathematical model of the muscle, introduced by Daerden, was reformulated. This model describes the shape of the muscle bulging at each contraction, and gives essential characteristics such as muscle traction and enclosed volume. The difference in the adapted mathematical model is seen in the formulation for the generated muscle force, which becomes dependent on the discrete number of high-tensile fibers used to contract the muscle.

In order to validate the theoretical traction function with the real force generation, static load tests on a specific muscle were carried out. It was found that the mathematical model gives a good approximation for the force function such that it can be used for dimensioning purposes. Additionally, a polynomial fit on the measured force data was carried out to provide a more accurate force estimate.

There is growing interest in the use of pneumatic artificial muscles for robotic applications due to their high power to weight ratio and the adaptable compliance. Two applications which incorporate the PPAM have been given. One is the biped Lucy, in which the adaptable joint compliance is used in order to exploit the natural dynamics of the system. Another application is a manipulator arm in which the compliance is very important since this manipulator is working in direct contact with an operator.

REFERENCES

1. C.-P. Chou and B. Hannaford, Measurement and modeling of McKibben pneumatic artificial muscles, *IEEE Trans. Robotics Automat.* **12**, 90–102 (1996).
2. F. Daerden, Conception and realization of pleated pneumatic artificial muscles and their use as compliant actuation elements, PhD thesis, Vrije Universiteit, Brussels (1999).
3. F. Daerden and D. Lefeber, The concept and design of pleated pneumatic artificial muscles, *Int. J. Fluid Power* **2**, 41–50 (2001).
4. G. B. Immega, ROMAC actuators for micro robots, in: *Proc. IEEE Micro Robotics and Teleoperators Workshop*, Hyannis, MA (1987).
5. H. A. Baldwin, Realizable models of muscle function, in: *Proc. 1st Rock Biomechanics Symp.*, New York, pp. 139–148 (1969).
6. N. Saga, T. Nakamura, J. Uehara and T. Iwada, Development of artificial muscle actuator reinforced by kevlar fiber, in: *Proc. IEEE Int. Conf. on Industrial Technology*, Bangkok, pp. 950–954 (2002).
7. H. F. Schulte, The characteristics of the McKibben artificial muscle, in: *The Application of External Power in Prosthetics and Orthotics*, Publ. 874, pp. 94–115, National Academy of Sciences–National Research Council, Lake Arrowhead (1961).
8. K. Inoue, Rubbertuators and applications for robotics, in: *Proc. 4th Int. Symp. on Robotics Research*, Santa Cruz, CA, pp. 57–63 (1987).
9. Shadow Robot Company, Design of a dextrous hand for advanced CLAWAR applications, in: *Proc. 6th Int. Conf. on Climbing and Walking Robots and the Support Technologies for Mobile Machines*, Catania, pp. 691–698 (2003).
10. Merlin Systems, *Merlin Actuators: Automation, Animatronics and Artificial Creatures* [*Brochure*], Merlin Systems (2003).
11. Festo, *Fluidic muscle MAS* [*Brochure*], Festo (2004).
12. T. Noritsugu and T. Tanaka, Application of Rubber Artificial Muscle Manipulator as a Rehabilitation Robot, *IEEE/ASME Trans. Mechatron.* **2**, 259–267 (1997).
13. T. Raparelli, G. Mattiazzo, S. Mauro and M. Velardocchia, Design and development of a pneumatic anthropomorphic hand, *J. Robotic Syst.* **17**, 1–15 (2000).
14. S. Eskiizmiler, B. Tondu and C. Darlot, Motor control of a limb segment actuated by artificial muscles, in: *Proc. 23th IEEE/EMBS Annu. Conf.*, Istanbul, pp. 865–868 (2001).
15. K. G. Klute, J. M. Czerniecki and B. Hannaford, Artificial muscles: actuators for biorobotic systems, *Int. J. Robotics Res.* **21**, 295–309 (2002).
16. K. Berns, J. Albiez, V. Kepplin and C. Hillenbrand, Airbug insect-like machine actuated by fluidic muscle, in: *Proc. 4th Int. Conf. on Climbing and Walking Robots, from Biology to Industrial Application*, Karlsruhe, pp. 237–244 (2001).
17. S. Davis, N. Tsagarakis, J. Canderle and D. Caldwell, Enhanced modelling and performance in braided pneumatic muscle actuators, *Int. J. Robotics Res.* **22**, 213–227 (2003).
18. D. A. Kingsley, R. D. Quinn and R. E. Ritzmann, A cockroach inspired robot with artificial muscles, in: *Proc. Int. Symp. on Adaptive Motion of Animal and Machines*, Kyoto (2003).
19. P. Pomiers, Modular robot arm based on pneumatic artificial rubber muscles (PARM), in: *Proc. 6th Int. Conf. on Climbing and Walking Robots and the Support Technologies for Mobile Machines*, Catania, pp. 879–886 (2003).
20. K. Kawashima, T. Sasaki, T. Miyata, M. Nakamura, N. Sekiguchi and T. Kagawa, Development of robot using pneumatic artificial rubber muscles to operate machinery, *J. Robotics Mechatron.* **16**, pp. 8–16 (2004).
21. M. Wisse, Essentials of dynamic walking: analysis and design of two-legged robots, PhD Thesis, Technische Universiteit, Delft (2004).

22. B. Verrelst, R. Van Ham, B. Vanderborght, F. Daerden, D. Lefeber and J. Vermeulen, The pneumatic biped 'Lucy' actuated with pleated pneumatic artificial muscles, *Autonomous Robots* **18**, 201–213 (2005).
23. M. Van Damme, F. Daerden and D. Lefeber, Design of a pneumatic manipulator in direct contact with an operator, in: *Proc. 35th Int. Symp. on Robotics*, Paris (2004).

ABOUT THE AUTHORS

Björn Verrelst (1972). Studied Mechanical Engineering at the Vrije Universiteit Brussel and graduated in 1996. He obtained a PhD in Applied Sciences in 2005. He is a Post-doc Researcher at the Vrije Universiteit Brussel. The focus of his research is the use of pneumatic artificial muscles in the walking biped Lucy for dynamically balanced walking and compliant actuation for robotic applications in general. During the period 2005/2006 he is conducting a 1-year JSPS Post-doc research at the National Institute for Advanced Industrial Science and Technology in Tsukuba, Japan.

Ronald Van Ham (1976). Studied Electro-Mechanical Engineering at the Vrije Universiteit Brussel and graduated in 1999. Since 1999 he has been a Researcher and Teaching Assistant at the Vrije Universiteit Brussel. The focus of his research is the development and use of adaptable compliant actuators, e.g., pneumatic artificial muscles in the walking biped Lucy, Maccepa.

Bram Vanderborght (1980). Studied Mechanical Engineering at the Vrije Universiteit Brussel and graduated in 2003. Since 2003 he has been a Researcher at the Vrije Universiteit Brussel, supported by the Fund for Scientific Research Flanders (Belgium). The focus of his research is the use of adaptable compliance of pneumatic artificial muscles in the dynamically balanced biped Lucy.

Dirk Lefeber (1956). Studied Civil Engineering at the Vrije Universiteit Brussel. He obtained a PhD in Applied Sciences in 1986. He is a Professor at the Department of Mechanical Engineering, Head of the Robotics and Multibody Mechanics Research Group, Vrije Universiteit Brussel. His research interests are new actuators with adaptable compliance, dynamically balanced robots, robot assistants, rehabilitation robotics and multibody dynamics.

Frank Daerden (1966). Studied Mechanical Engineering at the Vrije Universiteit Brussel. He obtained a PhD in Applied Sciences in 1999. He is a Research and Teaching Assistant at the Vrije Universiteit Brussel, 1991–1999. Doctor-Assistant at the Department of Mechanical Engineering, Vrije Universiteit Brussel since 1999, Visiting Professor since 2003.

Michaël Van Damme (1978). Studied Electrical Engineering at the Vrije Universiteit Brussel and graduated in 2001. He has been a Researcher and Teaching Assistant at the Vrije Universiteit Brussel since 2003. The focus of his research is the use of a robotic assistive device in direct contact with an operator.